Rapid Communications

Elevating the magnetic exchange coupling in the compressed antiferromagnetic axion insulator candidate $EuIn_2As_2$

F. H. Yu,[1] H. M. Mu,[1] W. Z. Zhuo,[1] Z. Y. Wang,[1] Z. F. Wang,[1] J. J. Ying,[1,*] and X. H. Chen[1,2,†]

[1]*Hefei National Laboratory for Physical Sciences at Microscale and Department of Physics, and CAS Key Laboratory of Strongly-Coupled Quantum Matter Physics, University of Science and Technology of China, Hefei, Anhui 230026, China*

[2]*Collaborative Innovation Center of Advanced Microstructures, Nanjing 210093, China*

(Received 2 August 2020; accepted 26 October 2020; published 5 November 2020)

The magnetic topological materials have attracted much attention recently for their potential realization of various novel quantum states. However, the onset of magnetization in these materials usually occurs at low temperatures, impeding further applications. Here, by means of high pressure, we have significantly increased the magnetic transition temperature in an antiferromagnetic axion insulator candidate $EuIn_2As_2$. Both crystal and magnetic structures remain the same with pressure up to 17 GPa. The Néel temperature can be monotonously increased from 16 K (ambient pressure) to 65 K (14.7 GPa). This is mainly attributed to the enhancement of intralayer ferromagnetic exchange coupling by pressure. With increasing pressure up to 17 GPa, a crystalline-to-amorphous phase transition occurs, which impedes further enhancement of the Néel temperature. Our results show that high pressure is an effective pathway to greatly enhance the magnetic transition temperature in topological materials. It is helpful for the realization of novel quantum states at elevated temperatures.

DOI: 10.1103/PhysRevB.102.180404

Topology incorporated with magnetism provides a fertile playground for realizing novel quantum states such as quantum anomalous Hall effect and axion insulator states [1–6], and has attracted tremendous attention for their potential application in electronic and spintronic devices. Introducing a spontaneous magnetization can open an exchange gap on the Dirac spectrum which is initially protected by the time-reversal symmetry. In principle, the realization of these novel quantum states is limited by the magnetic transition temperature [4,6,7]. Thus, elevating the magnetic transition temperature is crucial for future progress of electronic devices based on magnetic topological materials. For the axion insulator, it has been proposed to be a promising platform for exploring quantized topological magnetoelectric coupling and axion electrodynamics in condensed matter physics [8–10]. While axion insulating state has been realized in sandwiched magnetic topological insulator heterostructures and even layered $MnBi_2Te_4$ thin flakes [1,7], reports on the bulk intrinsic materials are still lacking up to now. Recently, an antiferromagnetic Zintl compound $EuIn_2As_2$ is predicted to be a bulk axion insulator [11–13].

$EuIn_2As_2$ crystallizes in the hexagonal $P6_3/mmc$ space group and contains layers of Eu^{2+} cations separated by $[In_2As_2]^{2-}$ layers along the crystallographic c axis as shown in Fig. 1(b). Previous transport and magnetic measurements on $EuIn_2As_2$ single crystals revealed an antiferromagnetic (AFM) transition with relatively low Néel temperature $T_N \sim 16$ K [14,15]. The intralayer exchange coupling among Eu^{2+} ions is ferromagnetic, while the interlayer coupling is antiferromagnetic, leading to A-type AFM order. By applying an external magnetic field, the AFM state can be tuned to fully polarized ferromagnetism and negative colossal magnetoresistance was observed [14]. Theoretical calculations have found that the nontrivial topological states are strongly correlated with the magnetic structure in $EuIn_2As_2$. When the magnetic moments are along the ab plane, it is predicted to be a topological crystalline insulator [11]. It becomes a high-order topological insulator if the magnetic moments align along the c axis [11]. The energy difference between these two magnetic structures is very small [11]. Experimentally, the spin orientations are determined to be along the ab plane [13]; however, it could be tuned under certain conditions. For example, the magnetism of a similar compound $EuCd_2As_2$ can be manipulated by tuning the level of band filling [16].

Pressure provides a clean method to directly tune the lattice parameters that are crucial for both the magnetic and topological properties of the material. In $EuIn_2As_2$, both the interlayer and intralayer magnetic exchange coupling could change dramatically under high pressure, possibly leading to a significant change of the magnetic transition temperature or magnetic structure. It is also interesting to check the topological state and its correspondence with magnetism under pressure in this material. Here, by using the high-pressure x-ray diffraction measurement, we find that the structure of $EuIn_2As_2$ remains the same up to 17 GPa but becomes amorphous at higher pressure. More importantly, we find that T_N monotonously increases until the crystalline structure collapses, and eventually reaches a maximum value of 65 K (about four times that of the T_N at ambient pressure) mainly due to the significant enhancement of intralayer ferromagnetic exchange coupling. In this pressure range, the magnetic structure remains unchanged.

*yingjj@ustc.edu.cn
†chenxh@ustc.edu.cn

 ©2020 American Physical Society

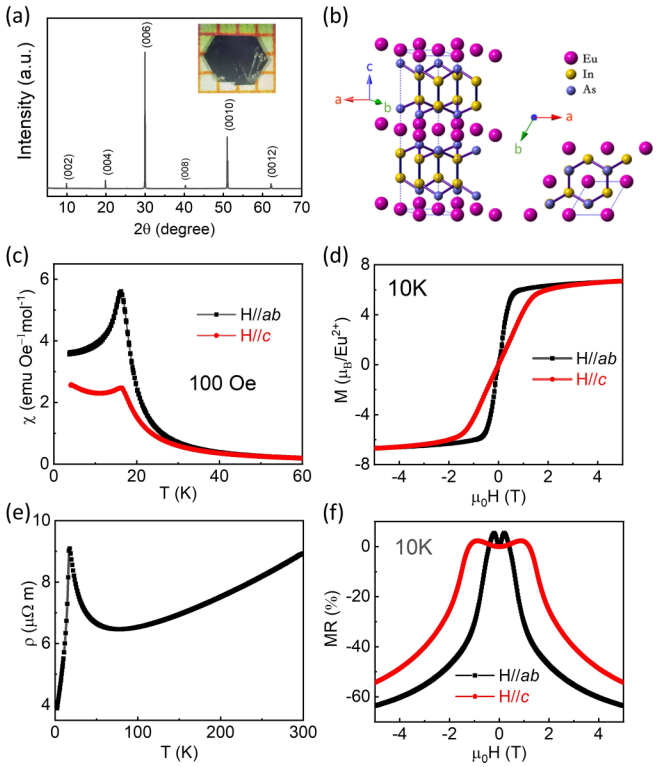

FIG. 1. (a) XRD pattern of $EuIn_2As_2$ single crystal with the corresponding Miller indices (00L) in parentheses. The inset represents an optical image of a typical $EuIn_2As_2$ single crystal. (b) Crystal structure of $EuIn_2As_2$ from different viewpoints (Eu, In, and As atoms are indicated as purple, yellow, and blue spheres, respectively). (c) Magnetic susceptibility as a function of temperature with applied field $H = 100$ Oe along different crystal directions for $EuIn_2As_2$ single crystal under ambient pressure. (d) Magnetic hysteresis loops (MH) with field applied along different crystallographic orientations at 10 K. (e) In-plane resistivity as a function of temperature for $EuIn_2As_2$ single crystal under ambient pressure. (f) Magnetoresistance curves with magnetic field applied along different crystal directions at 10 K.

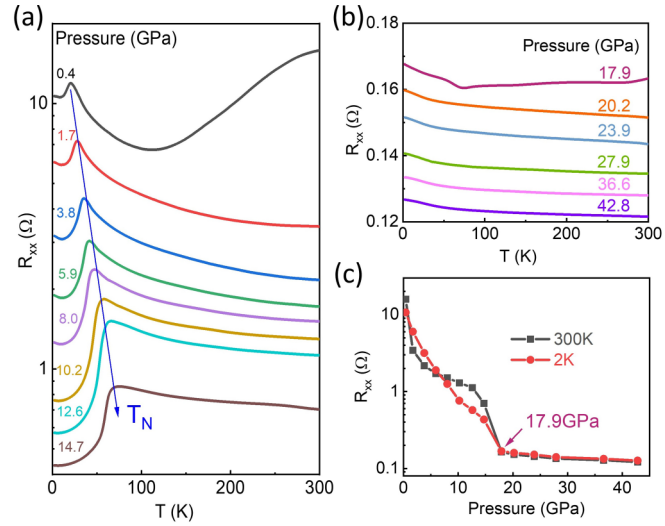

FIG. 2. (a) Temperature dependence of the in-plane electrical resistance (R_{xx}) for $EuIn_2As_2$ under various pressures below 17 GPa. The Néel temperature gradually increases with increasing the pressure. (b) Temperature dependences of the in-plane electrical resistivity for $EuIn_2As_2$ after phase transition. (c) Resistivity as a function of pressure for $EuIn_2As_2$ at 2 K (red circle) and 300 K (black square).

Our findings suggest that pressure is an effective method to elevate the magnetic transition temperature in magnetic topological materials, which is crucial for realizing the novel quantum states at higher temperatures.

We first check the ambient-pressure physical properties of $EuIn_2As_2$ single crystal before the high-pressure experiments. As indicated in Fig. 1(a), the x-ray diffraction (XRD) pattern represents sharp (00L) diffraction peaks, which are well consistent with the previous reports, indicating the pure phase of $EuIn_2As_2$. The inset of Fig. 1(a) shows an optical image of $EuIn_2As_2$ single crystal. We have performed magnetic and transport measurements at the ambient pressure and highlight the results in Figs. 1(c)–1(f). The magnetic susceptibility exhibits Curie Weiss behavior at high temperature and an antiferromagnetic transition around 16 K [Fig. 1(c)], similar to the previous reports. The resistivity of $EuIn_2As_2$ exhibits a metallic behavior at high temperature and a cusp around T_N due to the dramatic enhancement of magnetic fluctuations [Fig. 1(e)]. We have also checked the spin orientation of $EuIn_2As_2$ by performing isothermal magnetization and magnetoresistance (MR) measurements as indicated in Figs. 1(d) and 1(f), respectively. Magnetic field can gradually align the magnetic moment as evidenced by the M-H curves shown in Fig. 1(d). While a small magnetic field (about 0.7 T) can fully polarize the Eu moments in the ab plane, a much larger magnetic field (about 1.6 T) along the c axis is needed to fully polarize the spins, in consistency with the in-plane aligned moments reported previously [13]. The measured saturation moment (at 4 T) is 6.7 μ_B, slightly smaller than that expected for a single Eu^{2+} ion ($M_{sat} = 7.0\,\mu_B$). Figure 1(f) represents the isothermal magnetoresistance measured at 10 K. Below the saturation field, the MR for $EuIn_2As_2$ with $H||c$ slightly increases due to the enhancement of magnetic fluctuations. With magnetic fields above the saturation field, the MR starts to decrease dramatically since the system evolves into a ferromagnetic state in which the scatterings related to localized moments are suppressed giving rise to a negative MR. With $H||ab$, the system first enters a canted AFM state before the magnetic moments are fully polarized [13]. Quantitatively, we define H_{c1} (about 0.2 T) and H_{c2} (about 0.65 T) in the derivative of the MR curves (Fig. S1(a) in the Supplemental Material [17]) to describe these two transitions, where H_{c1} indicates an AFM to canted AFM transition while H_{c2} denotes the magnetic field above which the magnetic moments are fully polarized. As the magnetic field exceeds H_{c1}, the MR starts to decrease with increasing the magnetic field.

In order to investigate the physical properties of $EuIn_2As_2$ at high pressure, we first performed high-pressure resistance measurements as indicated in Fig. 2. The resistance gradually decreases with increasing the pressure as evidenced in Fig. 2(a). Interestingly, we find the anomaly associated with the antiferromagnetic transition gradually moves to higher temperature with increasing pressure. The resistance suddenly

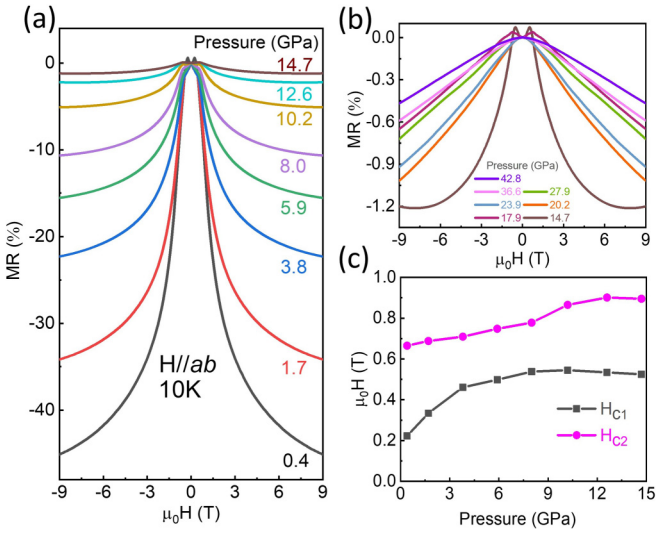

FIG. 3. (a), (b) Magnetoresistance of $EuIn_2As_2$ single crystal measured at 10 K under various pressures. (c) H_{c1} and H_{c2} as a function of pressure. The gradual increments of H_{c2} at high pressure indicating the slight enhancement of interlayer antiferromagnetic exchange coupling.

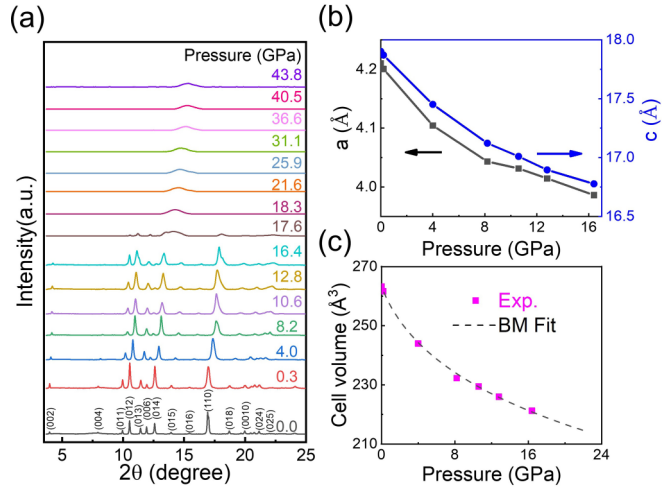

FIG. 4. (a) XRD patterns of $EuIn_2As_2$ under high pressure up to 43.8 GPa with an incident wavelength $\lambda = 0.6199$ Å. (b) Pressure dependence of the lattice parameters a and c for $EuIn_2As_2$. (c) The derived cell volume as a function of pressure for $EuIn_2As_2$. The black dotted line is a fitted curve by the Birch-Murnaghan equation of state with the derived bulk modulus $B_0 = 32.3$ GPa.

decreases when the pressure reaches 17 GPa as shown in Fig. 2(c), indicating a phase transition. The anomaly in the resistance disappears after the phase transition implying the absence of magnetic order in this new phase as indicated in Fig. 2(b). The sudden drop of Hall coefficient above 17 GPa (see Supplemental Material Fig. S2 [17]) further confirms a phase transition. The carrier type of $EuIn_2As_2$ is holelike and remains the same under high pressure. In this case, the sudden reduction of Hall coefficient in the high-pressure phase indicates an increment of carrier density after phase transition, consistent with the dramatic reduction of the resistance at high pressure. However, the resistance behavior exhibits weak upturn with the temperature decreases as shown in Fig. 2(b), possibly due to the disorder effect in the high-pressure phase.

In order to check whether the A-type AFM magnetic structure changes or not under pressure, we have performed the magnetoresistance measurements at 10 K with $H||ab$ under various pressures as represented in Fig. 3. The MR at low pressures show anomalies which are related to the magnetic transitions, similar to the ambient pressure results. By increasing the pressure, the magnitude of the MR gradually decreases. After the phase transition at 17 GPa, weak negative MR can be observed without any anomaly as shown in Fig. 3(b). We can derive H_{c1} and H_{c2} from the derivative of the MR curves before the phase transition (Fig. S1(b) in the Supplemental Material [17]). Figure 3(c) highlights the derived H_{c1} and H_{c2} as a function of pressure. Both the H_{c1} and H_{c2} evolve smoothly with pressure indicating the magnetic structure does not change at high pressure. H_{c2} slightly increases with increasing the pressure (H_{c2} at 14.7 GPa is about 30% higher than that at ambient pressure), indicating a slight increment of the interlayer antiferromagnetic exchange coupling constant; however, such small increment cannot explain the huge enhancement of T_N.

We also performed high-pressure XRD measurements on $EuIn_2As_2$ and summarized the results in Fig. 4. The XRD pattern at low pressure can be well indexed by using the hexagonal $P6_3/mmc$ space group. No structural phase transitions were observed below 17 GPa consistent with the transport measurements. We can derive the lattice parameters a and c under various pressures as indicated in Fig. 4(b). The extracted cell volume is shown in Fig. 4(c), which can be well fitted by the Birch-Murnaghan equation of state with a derived bulk modulus $B_0 = 32.3$ GPa. Above 17 GPa, the peaks suddenly disappear and a broad hump shows up in the XRD pattern, which indicates a crystalline-to-amorphous phase transition. Such phase transition was observed in many compounds at high pressure such as $Ge_2Sb_2Te_5$ [24] and $CrGeTe_3$ [25]. The amorphous phase exhibits lower resistivity and higher carrier density, compared with the crystalline phase. The weak insulating resistance behavior is possibly due to its structural disorder. By combing the high-pressure transport and XRD measurements, we can map out the phase diagram of $EuIn_2As_2$ as shown in Fig. 5(a). T_N monotonously increases by elevating the pressure, and reaches a maximum about 65 K at 14.7 GPa, which is about four times that of its ambient-pressure value. However, above 17 GPa, the system becomes amorphous, which impedes further increments of T_N.

To get a better physical understanding about the pressure-enhanced T_N in $EuIn_2As_2$, we have performed the first-principles calculations to investigate its high-pressure magnetic properties. The in-plane magnetization is set along the b axis within the ab plane. The nearest-neighbor intralayer (J_1, J_2) and interlayer (J_3) exchange couplings between Eu atoms are defined in the inset of Fig. 5(b), which are estimated through an energy mapping of the Heisenberg model [26] considering four different magnetic configurations in a $2\times2\times1$ supercell (see Supplemental Material Fig. S3 [17]). As indicated in Fig. 5(b), J_1 and J_2 monotonously increase

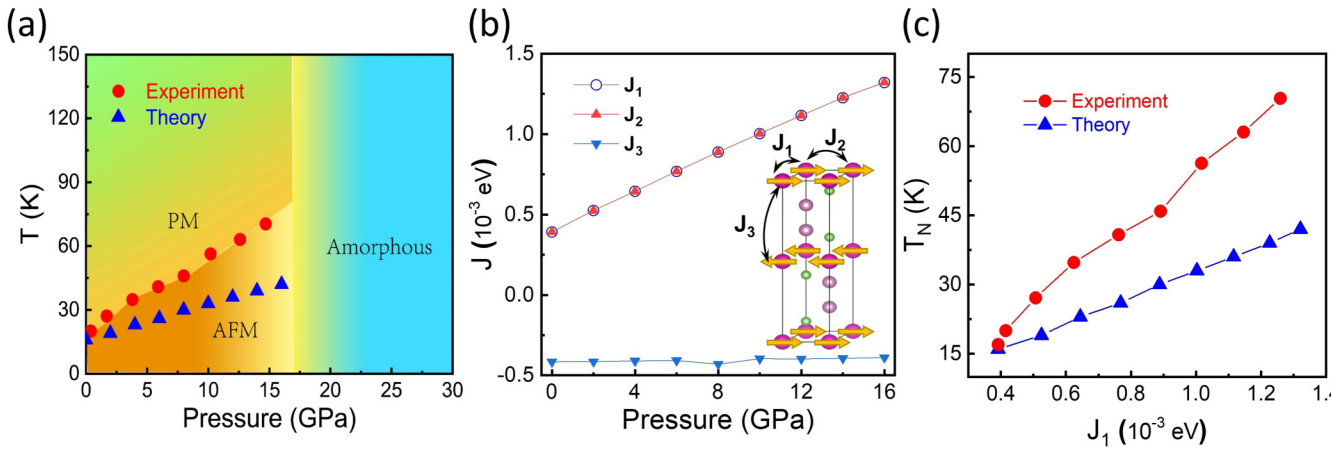

FIG. 5. (a) Pressure-temperature phase diagram of $EuIn_2As_2$. The red circle and blue triangle represent the Néel temperature T_N extracted from experimental and theoretical calculations, respectively. Above 17 GPa, the sample evolves into an amorphous phase. (b) Calculated exchange coupling parameters as a function of pressure. The intralayer coupling J_1 and J_2 gradually increases with increasing the pressure; however, the interlayer coupling J_3 remains the same under pressure. The inset is the definition of nearest-neighbor exchange coupling. (c) The Néel temperature as a function of the intralayer coupling J_1.

with increasing the pressure, while J_3 shows little change. Furthermore, we used Monte Carlo simulations with periodic boundary in the framework of the Ising model to estimate the T_N under different pressures. Once reaching the equilibrium state at a target temperature, the T_N can be extracted from the peak of specific capacity curves (see Supplemental Material Fig. S4 [17]). As represented in Fig. 5(a), the estimated T_N monotonously increases with increasing pressure, from 16 K (ambient pressure) to 42 K (16 GPa), which is comparable to the experimental observations. The calculated T_N is linearly dependent with the exchange coupling constant J_1 as shown in Fig. 5(c). Therefore, our first-principles calculations demonstrate that the pressure-enhanced T_N in $EuIn_2As_2$ can be attributed to the pressure-enhanced intralayer exchange coupling, while interlayer exchange coupling has negligible contribution. Since the calculated and measured T_N's at 0 GPa are consistent with each other, this indicates a reliable parameter setup of our calculations at ambient pressure. However, the Hubbard U is fixed in our high-pressure calculations. We found that if we used linear decreasing of Hubbard U with the increasing of pressure, one can find good agreement between experimental and theoretical data by including such a Hubbard-U correction (see Supplemental Material Fig. S5 [17]). Therefore, the discrepancy between the calculated and measured T_N is possibly due to the variation of Hubbard U under pressure, which can result in an underestimation of the exchange coupling parameter at high pressure.

In many magnetic samples, pressure usually suppresses the magnetic transition temperature and/or magnetic moment [27,28]. For the compounds with Eu^{2+} ions, the valence transition from magnetic Eu^{2+} to nonmagnetic Eu^{3+} is expected at high pressure since the ion radius of Eu^{3+} is smaller than Eu^{2+} [29]. Therefore, high pressure tends to weaken the magnetism in Eu-based compounds. In fact, such valence transition has been observed in $EuFe_2As_2$ [30] and $EuRh_2Si_2$ [31]. In our case, the Eu^{2+} to Eu^{3+} valence transition is absent below 17 GPa; instead the intralayer ferromagnetic exchange coupling constant gets greatly enhanced due to the reduction of the in-plane distances under high pressure, which would lead to the giant enhancement of T_N. The giant enhancement of magnetic transition temperature under pressure is rather rare and crucial for realizing the novel quantum states in magnetic topological materials. However, further increasing the pressure, the crystal structure becomes unstable and the system evolves to an amorphous phase. We cannot detect any magnetic phase transitions in the amorphous phase, and it is interesting to check whether the structural transition is accompanied with the Eu^{2+} to Eu^{3+} valence transition in the future. An isostructural compound $EuIn_2P_2$ exhibits a similar magnetic property as $EuIn_2As_2$ and has a slightly higher magnetic transition temperature around 24 K [32], indicating the chemical pressure can also enhance T_N but with a less efficient way comparing with the external pressure. The magnetic structure and transition temperature are intimately related to the inter- and intralayer exchange coupling constant, thus the magnetic structure can be possibly tuned in the other magnetic topological materials under pressure, leading to a pressure-induced topological phase transition. Considering a continuously increasing number of magnetic topological materials, it would be interesting to check their magnetic properties under pressure in the future.

In conclusion, we have systematically investigated the high-pressure properties of $EuIn_2As_2$ single crystal. We found a crystalline-to-amorphous phase transition around 17 GPa. The sample keeps its initial AFM magnetic structure below the transition pressure; however, T_N is greatly enhanced due to the increment of intralayer ferromagnetic exchange coupling constant at high pressure. Our results indicate high pressure is an effective method to enhance the magnetic transition temperature, which is crucial for realizing novel quantum states in the future.

This work was supported by the National Key Research and Development Program of the Ministry of Science and Technology of China (Grants No. 2019YFA0704900, No. 2016YFA0300201, No. 2017YFA0303001, and No. 2017YFA0204904), the National Natural Science Foundation of China (Grants No. 11888101, No. 11534010, No. 11774325, and No. 21603210), the Strategic Priority

Research Program of Chinese Academy of Sciences (Grant No. XDB25000000), Anhui Initiative in Quantum Information Technologies (Grant No. AHY160000), the Science Challenge Project of China (Grant No. TZ2016004), the Key Research Program of Frontier Sciences, CAS, China (Grant No. QYZDYSSW-SLH021), and Fundamental Research Funds for the Central Universities (Grants No. WK3510000011, No. WK2030020031, and No. WK3510000007). High-pressure synchrotron XRD work was performed at the BL15U1 beamline, Shanghai Synchrotron Radiation Facility (SSRF) in China. We also thank Supercomputing Center at USTC for providing the computing resources.

[1] M. Mogi, M. Kawamura, R. Yoshimi, A. Tsukazaki, Y. Kozuka, N. Shirakawa, K. S. Takahashi, M. Kawasaki, and Y. Tokura, Nat. Mater. **16**, 516 (2017).
[2] Z. Feng, J. Yuan, G. He, W. Hu, Z. Lin, D. Li, X. Jiang, Y. Huang, S. Ni, J. Li, B. Zhu, X. Dong, F. Zhou, H. Wang, Z. Zhao, and K. Jin, Sci. Rep. **8**, 4039 (2018).
[3] R. Yu, W. Zhang, H.-J. Zhang, S.-C. Zhang, X. Dai, and Z. Fang, Science **329**, 61 (2010).
[4] C.-Z. Chang, J. Zhang, X. Feng, J. Shen, Z. Zhang, M. Guo, K. Li, Y. Ou, P. Wei, L.-L. Wang *et al.*, Science **340**, 167 (2013).
[5] Y. Tokura, K. Yasuda, and A. Tsukazaki, Nat. Rev. Phys. **1**, 126 (2019).
[6] Y. Deng, Y. Yu, M. Z. Shi, Z. Guo, Z. Xu, J. Wang, X. H. Chen, and Y. Zhang, Science **367**, 895 (2020).
[7] C. Liu, Y. Wang, H. Li, Y. Wu, Y. Li, J. Li, K. He, Y. Xu, J. Zhang, and Y. Wang, Nat. Mater. **19**, 522 (2020).
[8] X.-L. Qi, T. L. Hughes, and S.-C. Zhang, Phys. Rev. B **78**, 195424 (2008).
[9] F. Wilczek, Phys. Rev. Lett. **58**, 1799 (1987).
[10] A. M. Essin, J. E. Moore, and D. Vanderbilt, Phys. Rev. Lett. **102**, 146805 (2009).
[11] Y. Xu, Z. Song, Z. Wang, H. Weng, and X. Dai, Phys. Rev. Lett. **122**, 256402 (2019).
[12] S. Regmi, M. Mofazzel Hosen, B. Ghosh, B. Singh, G. Dhakal, C. Sims, B. Wang, F. Kabir, K. Dimitri, Y. Liu *et al.*, Phys. Rev. B **102**, 165153 (2020).
[13] Y. Zhang, K. Deng, X. Zhang, M. Wang, Y. Wang, C. Liu, J.-W. Mei, S. Kumar, E. F. Schwier, K. Shimada *et al.*, Phys. Rev. B **101**, 205126 (2020).
[14] A. M. Goforth, P. Klavins, J. C. Fettinger, and S. M. Kauzlarich, Inorg. Chem. **47**, 11048 (2008).
[15] P. F. S. Rosa, C. Adriano, T. M. Garitezi, R. A. Ribeiro, Z. Fisk, and P. G. Pagliuso, Phys. Rev. B **86**, 094408 (2012).
[16] N. H. Jo, B. Kuthanazhi, Y. Wu, E. Timmons, T.-H. Kim, L. Zhou, L.-L. Wang, B. G. Ueland, A. Palasyuk, D. H. Ryan *et al.*, Phys. Rev. B **101**, 140402 (2020).
[17] See Supplemental Material at http://link.aps.org/supplemental/10.1103/PhysRevB.102.180404 for further details on the experimental measurements and first-principles calculations, as well as Figs. S1–S5, and Refs. [14,18–23].
[18] H. K. Mao, J. Xu, and P. M. Bell, J. Geophys. Res.: Solid Earth **91**, 4673 (1986).
[19] A. G. Gavriliuk, A. A. Mironovich, and V. V. Struzhkin, Rev. Sci. Instrum. **80**, 043906 (2009).
[20] G. Kresse and D. Joubert, Phys. Rev. B **59**, 1758 (1999).
[21] J. P. Perdew, K. Burke, and M. Ernzerhof, Phys. Rev. Lett. **77**, 3865 (1996).
[22] P. E. Blöchl, Phys. Rev. B **50**, 17953 (1994).
[23] S. L. Dudarev, G. A. Botton, S. Y. Savrasov, C. J. Humphreys, and A. P. Sutton, Phys. Rev. B **57**, 1505 (1998).
[24] Z. Sun, J. Zhou, Y. Pan, Z. Song, H.-K. Mao, and R. Ahuja, Proc. Natl. Acad. Sci. USA **108**, 10410 (2011).
[25] Z. Yu, W. Xia, K. Xu, M. Xu, H. Wang, X. Wang, N. Yu, Z. Zou, J. Zhao, L. Wang *et al.*, J. Phys. Chem. C **123**, 13885 (2019).
[26] H. Xiang, C. Lee, H.-J. Koo, X. Gong, and M.-H. Whangbo, Dalton Trans. **42**, 823 (2013).
[27] H. V. Löhneysen, A. Rosch, M. Vojta, and P. Wölfle, Rev. Mod. Phys. **79**, 1015 (2007).
[28] J. Ying, H. Lei, C. Petrovic, Y. Xiao, and V. V. Struzhkin, Phys. Rev. B **95**, 241109(R) (2017).
[29] Y. Ōnuki, A. Nakamura, F. Honda, D. Aoki, T. Tekeuchi, M. Nakashima, Y. Amako, H. Harima, K. Matsubayashi, Y. Uwatoko *et al.*, Philos. Mag. **97**, 3399 (2017).
[30] K. Matsubayashi, K. Munakata, M. Isobe, N. Katayama, K. Ohgushi, Y. Ueda, Y. Uwatoko, N. Kawamura, M. Mizumaki, N. Ishimatsu, M. Hedo, I. Umehara, and Y. Uwatoko, Phys. Rev. B **84**, 024502 (2011).
[31] A. Mitsuda, S. Hamano, N. Araoka, H. Yayama, and H. Wada, J. Phys. Soc. Jpn. **81**, 023709 (2012).
[32] J. Jiang and S. M. Kauzlarich, Chem. Mater. **18**, 435 (2006).